◆ Human Brain Mapping 30:1511–1523 (2009) ◆

Parcellation-Dependent Small-World Brain Functional Networks: A Resting-State fMRI Study

Jinhui Wang,[1†] Liang Wang,[1,2†] Yufeng Zang,[1] Hong Yang,[3] Hehan Tang,[3] Qiyong Gong,[3] Zhang Chen,[4] Chaozhe Zhu,[1*] and Yong He[1,4*]

[1]*State Key Laboratory of Cognitive Neuroscience and Learning, Beijing Normal University, Beijing, China*
[2]*School of Information Science and Technology, Beijing Institute of Technology, Beijing, China*
[3]*Huaxi MR Research Center, Department of Radiology, West China Hospital of Sichuan University, Chengdu, China*
[4]*McConnell Brain Imaging Centre, Montreal Neurological Institute, McGill University, Montreal, Quebec, Canada*

Abstract: Recent studies have demonstrated small-world properties in both functional and structural brain networks that are constructed based on different parcellation approaches. However, one fundamental but vital issue of the impact of different brain parcellation schemes on the network topological architecture remains unclear. Here, we used resting-state functional MRI (fMRI) to investigate the influences of different brain parcellation atlases on the topological organization of brain functional networks. Whole-brain fMRI data were divided into ninety and seventy regions of interest according to two predefined anatomical atlases, respectively. Brain functional networks were constructed by thresholding the correlation matrices among the parcellated regions and further analyzed using graph theoretical approaches. Both atlas-based brain functional networks were found to show robust small-world properties and truncated power-law connectivity degree distributions, which are consistent with previous brain functional and structural networks studies. However, more importantly, we found that there were significant differences in multiple topological parameters (e.g., small-worldness and degree distribution) between the two groups of brain functional networks derived from the two atlases. This study provides quantitative evidence on how the topological organization of brain networks is affected by the different parcellation strategies applied. *Hum Brain Mapp 30:1511–1523, 2009.* **© 2008 Wiley-Liss, Inc.**

Key words: parcellation; atlas; small-world; brain networks; fMRI; resting-state; efficiency

[†]Jinhui Wang and Liang Wang contributed equally to this work.

Contract grant sponsor: National Natural Science Foundation (NSFC) of China; Contract grant numbers: 30625024, 30728017, 30700256, 30621130074; Contract grant sponsor: National Key Basic Research and Development Program (973 Program); Contract grant numbers: 2003CB716101, 2007CB512305; Contract grant sponsor: UK Royal Society International Joint Project with NSFC; Contract grant numbers: 30530300, 2006/R3; Contract grant sponsor: High Technology Program of China (863 Program); Contract grant number: 2007AA02Z430.

*Correspondence to: Yong He, PhD, State key Laboratory of Cognitive Neuroscience and Learning, Beijing Normal University, 100875, Beijing, China. E-mail: yong.he@bnu.edu.cn or Chaozhe Zhu, PhD, State key Laboratory of Cognitive Neuroscience and Learning, Beijing Normal University, 100875, Beijing, China. E-mail: czzhu@bnu.edu.cn

Received for publication 23 January 2008; Revised 14 April 2008; Accepted 12 May 2008

DOI: 10.1002/hbm.20623

Published online 22 July 2008 in Wiley InterScience (www.interscience.wiley.com).

INTRODUCTION

Many complex networks such as social, economical, and biological networks have been found to exhibit small-world attributes characterized by dense local interconnectivity but short characteristic path lengths linking individual network nodes (Watts and Strogatz, 1998; for a review, see Boccaletti et al., 2006). For the characterization of complex brain networks, the small-world is also an attractive model because the combination of high local clustering and short paths supports the two fundamental organizational principles in the brain: functional segregation and functional integration (for reviews, see Bassett and Bullmore, 2006; Stam and Reijneveld, 2007). Previous studies have demonstrated the small-world topology in both human brain structural (Hagmann et al., 2007; He et al., 2007; Itturia-Medina et al., 2007) and functional networks (Achard and Bullmore, 2007; Achard et al., 2006; Bassett et al., 2006; Stam 2004). Moreover, the small-world network model has been employed to investigate the changes in the coordinated patterns of large-scale brain functional networks in patients with brain diseases (De Vico Fallani et al., 2007; Liu et al., 2008; Ponten et al., 2007; Rubinov et al., in press; Stam et al., 2007; Wang et al., in press). These advances in complex brain networks research provide new insights into the relationship between network organization and functional activities under normal and pathological conditions.

Although the attractive small-world approach opens new opportunities for the researches on brain networks, there are some fundamental issues (for reviews, see Bassett and Bullmore, 2006; Sporns et al., 2005) that need to be elucidated. One of the main concerns is the differences in the definition of network nodes in terms of the electrodes in electroencephalograph (EEG), magnetic channels in magnetoencephalograph (MEG), or brain regions derived from the anatomical atlases in structural and functional MRI (sMRI/fMRI). For example, researchers have constructed large-scale brain networks using 19 (Ferri et al., 2007), 21 (Ponten et al., 2007; Stam et al., 2007), and 28 (Micheloyannis et al., 2006a,b) electrodes from EEG data; 126 (Stam, 2004) and 275 (Bassett et al., 2006) channels from MEG data; 54 anatomical regions from sMRI (He et al., 2007, 2008) and 90 anatomical regions from fMRI (Achard et al., 2006; Achard and Bullmore, 2007; Liu et al., 2008; Salvador et al., 2005; Wang et al., in press). Node definition is vital during the brain network analysis, since the node is the most essential element of a network (Sporns et al. 2005). However, little is known about the impact of different network node definitions on the topological architecture of the networks.

The present study aimed to investigate the effects of different brain parcellation schemes (different node characterization) on the topological architecture of human brain functional networks. To address this issue, we analyzed and compared two groups of parcellation-dependent brain functional networks obtained from the same resting-state functional MRI (fMRI) dataset. The spontaneous low-frequency fluctuations measured by resting-state fMRI are highly synchronized between multiple brain regions, which can be used to investigate the coordinated patterns of large-scale brain functional networks (for a review, see Fox et al., 2007). Two popular predefined parcellation atlases applied in the study are the Automated Anatomical Labelling (AAL) (Tzourio-Mazoyer et al., 2002) and Automatic Nonlinear Imaging Matching and Anatomical Labelling (ANIMAL) (Collins et al., 1995; Kabani et al., 1998), both of which have been widely used in large-scale human brain networks studies (for AAL-atlas: Achard et al., 2006; Achard and Bullmore, 2007; Liu et al., 2008; Salvador et al., 2005; Wang et al., in press; for ANIMAL-atlas: Chen et al., in press; He et al., 2007, 2008) (for the detailed description of the two atlases, see "Discussion"). Notably, it is crucial to apply different atlases to a single dataset and compare the resulting network topology attributes to control variations caused by different subjects, scanner parameters, and data preprocessing. In this study, we first measured functional connectivity (Friston et al., 1993) between any pair of brain regions (defined by the two different brain atlases) by calculating Pearson correlations between the time series of the regions. For each subject, two inter-regional correlation matrices were then obtained and further thresholded into a set of binarized matrices underlying the topological organization of brain functional networks. Finally, small-world properties and degree distribution of the two atlases-based brain functional networks were quantified and the differences between the corresponding topological parameters were further statistically evaluated.

MATERIALS AND METHODS

Subjects

Eighteen right-handed healthy volunteers (nine males and nine females, 21–25 years) were recruited from Sichuan University. All subjects had no history of neurological or psychiatric disorders. Written informed consent was obtained from each participant and this study was approved by the Ethics Committee of Huaxi Hospital, Sichuan University.

Data Acquisitions

All subjects were scanned on a 3.0 Tesla GE MR scanner (EXCITE, Milwaukee, USA) in Huaxi MR Research Center (HMRRC) at the West China Hospital of Sichuan University. Foam pads and headphones were used to reduce head motion and scanner noise. Functional images were obtained using an echo-planar imaging (EPI) sequence: 30 axial slices, thickness/gap = 4.5/0 mm, matrix = 64 × 64, repetition time = 2,000 ms, echo time = 30 ms, flip angle = 90°, field of view = 220 × 220 mm^2. Subjects were instructed to keep their eyes closed, relax their minds, and remain motionless

TABLE I. Regions of interest included in AAL-atlas

Regions	Abbreviations	Regions	Abbreviations
Precentral gyrus	PreCG	Lingual gyrus	LING
Superior frontal gyrus (dorsal)	SFGdor	Superior occipital gyrus	SOG
Orbitofrontal cortex (superior)	ORBsup	Middle occipital gyrus	MOG
Middle frontal gyrus	MFG	Inferior occipital gyrus	IOG
Orbitofrontal cortex (middle)	ORBmid	Fusiform gyrus	FFG
Inferior frontal gyrus (opercular)	IFGoperc	Postcentral gyrus	PoCG
Inferior frontal gyrus (triangular)	IFGtriang	Superior parietal gyrus	SPG
Orbitofrontal cortex (inferior)	ORBinf	Inferior parietal lobule	IPL
Rolandic operculum	ROL	Supramarginal gyrus	SMG
Supplementary motor area	SMA	Angular gyrus	ANG
Olfactory	OLF	Precuneus	PCUN
Superior frontal gyrus (medial)	SFGmed	Paracentral lobule	PCL
Orbitofrontal cortex (medial)	ORBmed	Caudate	CAU
Rectus gyrus	REC	Putamen	PUT
Insula	INS	Pallidum	PAL
Anterior cingulate gyrus	ACG	Thalamus	THA
Middler cingulate gyrus	MCG	Heschl gyrus	HES
Posterior cingulate gyrus	PCG	Superior temporal gyrus	STG
Hippocampus	HIP	Temporal pole (superior)	TPOsup
Parahippocampal gyrus	PHG	Middle temporal gyrus	MTG
Amygdala	AMYG	Temporal pole (middle)	TPOmid
Calcarine cortex	CAL	Inferior temporal gyrus	ITG
Cuneus	CUN		

as much as possible during the EPI data acquisition. The scan lasted for 400 s. For each subject, the first ten volumes were discarded to allow for T1 equilibration effects and the adaptation of the subjects to the circumstances, leaving 190 volumes for further analysis.

Data Preprocessing

Image preprocessing was carried out using the SPM5 package (http://www.fil.ion.ucl.ac.uk/spm). First, all functional images were corrected for the acquisition time delay between slices of each volume using the sinc interpolation and for the geometrical displacement due to head movement using a six-parameter (rigid body) spatial transformation (Friston et al., 1995). No dataset was excluded according to the criteria that head motion was less than 1 mm of displacement or 1 degree of rotation in any direction. After the correction, the images were normalized into the stereotaxic space (Talairach and Tournoux, 1988) using an optimum 12-parameter affine transformation and nonlinear deformations (Ashburner and Friston, 1999), and then resampled to 3-mm isotropic voxels. Given that the spontaneous synchrony of the bold oxygen level-dependent (BOLD) signal of fMRI is predominantly subtended by very low frequency signal components (Biswal et al., 1995; Kiviniemi et al., 2000; Lowe et al., 1998), the resulting data were further temporally band-pass filtered (0.01–0.1 Hz) to reduce the effects of low-frequency drift and high-frequency physiological noises.

Correlation Matrix and Graph Construction

To define the brain regions, each brain was first parcellated into 90 regions of interest (ROIs) using the AAL-atlas (45 for each hemisphere, see Table I) and 70 ROIs (35 for each hemisphere, see Table II) using the ANIMAL-atlas, respectively. The mean time series of each region was then acquired by averaging the time series of all voxels within that region. Several sources of spurious variances arising from estimated head-motion profiles and global signal activity (Fox et al., 2005; Wang et al., in press) were further removed by multiple linear regression analysis. The residual of this regression was then used to substitute for the raw mean time series of the corresponding regions. To measure the functional connectivity among regions, we calculated the Pearson correlation coefficients between any possible pair of regional residual time series, and then obtained two correlation matrices (90×90 for AAL-atlas and 70×70 for ANIMAL-atlas) for each subject. Finally, each correlation matrix was thresholded by a pre-selected threshold value (see below for details) to obtain a undirected binarized graph (network), in which nodes represent brain regions and edges represent links between regions. The networks were further analyzed by using graph theoretical approaches. All topological parameters of the brain networks calculated in this study and their implications were presented in Table III.

Small-World Properties

Conventional small-world measurements

Small-world parameters of a network (clustering coefficient, C_p, and characteristic path length, L_p) were originally proposed by Watts and Strogatz (1998). The C_p of a network is the average of the clustering coefficients over all

TABLE II. Regions of interest included in ANIMAL-atlas

Regions	Abbreviations	Regions	Abbreviations
Superior frontal gyrus	SFG	Lateral occipitotemporal gyrus	LOTG
Middle frontal gyrus	MFG	Parahippocampal gyrus	PHG
Inferior frontal gyrus	IFG	Insula	INS
Medial frontal gyrus	MdFG	Occipital pole	OP
Precentral gyrus	PrCG	Superior occipital gyrus	SOG
Lateral fronto-orbital gyrus	LOFG	Middle occipital gyrus	MOG
Medial front-orbital gyrus	MOFG	Inferior occipital gyrus	IOG
Cingulate region	CING	Cuneus	CUN
Superior parietal lobule	SPL	Lingual gyrus	LING
Supramarginal gyrus	SMG	Caudate nucleus	CAU
Angular gyrus	ANG	Putamen	PUT
Precuneus	PCU	Globus palladus	GP
Postcentral gyrus	PoCG	Thalamus	THA
Superior temporal gyrus	STG	Amygdala	AMYG
Middle temporal gyrus	MTG	Hippocampal formation	HIP
Inferior temporal gyrus	ITG	Nucleus accumbens	NA
Uncus	UNC	Subthalamic nucleus	SUBT
Medial occipitotemporal gyrus	MOTG		

nodes, where the clustering coefficient of a node ($C_{p\text{-nodal}}$) is defined as the ratio of the number of existing connections among the node's neighbors and all their possible connections. C_p quantifies the local interconnectivity of a graph. The L_p of a graph is the minimal number of edges required to link one node to another, averaged overall all pair of nodes. L_p is an indicator of overall routing efficiency of a graph. In this study, we calculated L_p as the "harmonic mean" distance between all possible pairs of regions (Newman, 2003) to deal with the disconnected graphs dilemma. To estimate the small-world properties, we generated 100 degree-matched random networks (Maslov and Sneppen, 2002; Sporns and Zwi, 2004) and scaled the C_p and L_p of the real networks with the mean $C_{p\text{-}s}$ and $L_{p\text{-}s}$ of all the random networks (i.e., $C_p/C_{p\text{-}s}$ and $L_p/L_{p\text{-}s}$). Typically, a small-world network should fulfill the following conditions: $C_p/C_{p\text{-}s} > 1$ and $L_p/L_{p\text{-}s} \approx 1$ (Watts and Strogatz, 1998). These conventional measures have been recently applied to many structural and functional brain networks studies (Achard et al., 2006; Achard

TABLE III. Topological parameters of brain functional networks used in this study

Network properties	Characters	Descriptions
Small-world properties	C_p	The clustering coefficient of a network that is the average of the clustering coefficient, $C_{p\text{-nodal}}$, over all nodes. It measures the extent of local cluster or cliquishness of the network.
	L_p	The characteristic path length of a network that is the average minimum number of connections linking any two nodes of the network. It measures the extent of overall routing efficiency of the network.
	E_{loc}	The local efficiency of a network that is the average of the local efficiency, $E_{loc\text{-nodal}}$, over all nodes. It measures the mean local efficiency of the network.
	E_{glob}	The global efficiency of a network that is the inverse of the harmonic mean of the minimum path length between any two nodes. It measures the extent of information propagation through the whole network.
	S, K	The sparsity or the cost to build a network.
Degree distribution	a	A scalar parameter, which reflects the extent that the node degree spans within a network.
	k_c	A cutoff value, which evaluates the extent of an exponential decay.
Nodal properties	k_{nodal}	The number of edges linking a single node.
	$C_{p\text{-nodal}}$	The nodal clustering coefficient that measures the extent of interconnectivity among the neighbors of the node.
	$E_{loc\text{-nodal}}$	The nodal local efficiency that measures the extent of information transmission among the neighbors of the node.
	E_{nodal}	The nodal global efficiency that measures the extent of information transmission of the node with all other nodes in the network.

and Bullmore 2007; He et al., 2007; Ponten et al., 2007; Stam et al., 2007).

Small-world efficiency measurements

In addition to the conventional small-world parameters (C_p and L_p) abovementioned, a more biologically sensible property of brain networks is the network efficiency that can be described in terms of global efficiency (E_{glob}) and local efficiency (E_{loc}) (Latora and Marchiori, 2001). For a graph G with N nodes,

$$E_{glob}(G) = \frac{1}{N}\sum_{i\in G} E_{nodal}(i)$$

where

$$E_{nodal}(i) = \frac{1}{N-1}\sum_{j\neq i\in G}\frac{1}{L_{i,j}}$$

with $L_{i,j}$ denoting the minimal number of edges required to go from node i to node j;

$$E_{loc}(G) = \frac{1}{N}\sum_{i\in G} E_{loc-nodal}(i)$$

where

$$E_{loc-nodal}(i) = E_{glob}(G_i)$$

with G_i denoting the subgraph composed of the nearest neighbors of node i. Global efficiency (E_{glob}) and local efficiency (E_{loc}) of a network measure the ability of information transmission of the network at the global and local level, respectively. The efficiency metric has a number of technical and conceptual advantages over conventional C_p and L_p measures, since it can (i) represent how efficiently a network exchanges local and global information by a single measure, and (ii) deal with either the disconnected or nonsparse graphs or both (Bassett and Bullmore, 2006; Latora and Marchiori, 2001). Very recently, this metric has been applied to human brain functional (Achard and Bullmore, 2007; De Vico Fallani et al., 2007; Wang et al., in press) and structural (Iturria-Medina et al., 2008) network studies. In this study, we also investigated the ratios of local efficiency ($E_{loc}/E_{loc\text{-}s}$) and global efficiency ($E_{glob}/E_{glob\text{-}s}$) between the real brain functional networks and 100 degree-matched random networks to assess small-world properties of brain functional networks. Typically, a small-world network has a higher local efficiency than its random counterparts ($E_{loc}/E_{loc\text{-}s} > 1$) and an approximately equivalent global efficiency ($E_{glob}/E_{glob\text{-}s} \approx 1$).

Degree Distribution

Recent studies have found that small-world brain networks follow different connectivity degree distribution such as power law (Eguiluz et al., 2005), exponential (Hagmann et al., 2007), and exponentially truncated power law distribution (Achard et al., 2006; He et al., 2007; Iturria-Medina et al., 2008; Wang et al., in press), where degree of a node (k_{nodal}) is the number of edges linking the node. The networks with different categories of degree distribution exhibited specific behaviors such as the robustness against hub attacks (Albert et al., 2000; Amaral et al., 2000; Achard et al., 2006). Given the fact that these brain networks were constructed at different spatial scales (e.g. voxel- or region-based level), thus we hypothesized that the different pacellation schemes used in this study could be associated with different degree distributions.

Statistical Analysis

Threshold selection

The selection of threshold is critical to make the topological measures between the two groups of networks with different size (90 vs. 70) comparable. In this study, we chose the sparsity, S, and wiring cost, K, of the brain networks (number of existing edges over the maximum possible number of edges) as threshold measurements for the between-group comparisons of the small-world parameters. By assigning both groups of brain networks with the same S or K, we excluded the effects of low-level correlation discrepancies on topological architecture. Given the fact that the selection of different threshold values could cause the changes in small-world network parameters, we therefore examined the between-group differences in topological parameters of functional brain networks over a wide range of threshold level, $0.05 \leq S, K \leq 0.5$, where the small-world attributes are estimable (Watts and Strogatz, 1998), and the resulting matrices have sparse properties (Achard et al., 2006; Achard and Bullmore, 2007; He et al., 2007; Wang et al., in press).

Statistical comparisons

To determine whether there existed significant differences in topological properties of brain functional networks between the two groups, in this study, paired t tests were performed on all small-world parameters (C_p, L_p, $C_p/C_{p\text{-}s}$, $L_p/L_{p\text{-}s}$, E_{loc}, E_{glob}, $E_{loc}/E_{loc\text{-}s}$ and $E_{glob}/E_{glob\text{-}s}$) at each threshold ($S$ and K) level. P values less than 0.05 (corrected by Bonferroni method for multiple comparisons) were considered significantly different between the two groups. Energies of the network parameters [i.e. the areas under the curves of all small-world parameters (Achard and Bullmore, 2007)] were also evaluated as the summarized measures of the networks over a preselected range of S and K followed by paired t tests. In addition, the fitting parameters of degree distribution were also compared between the two groups at several threshold values.

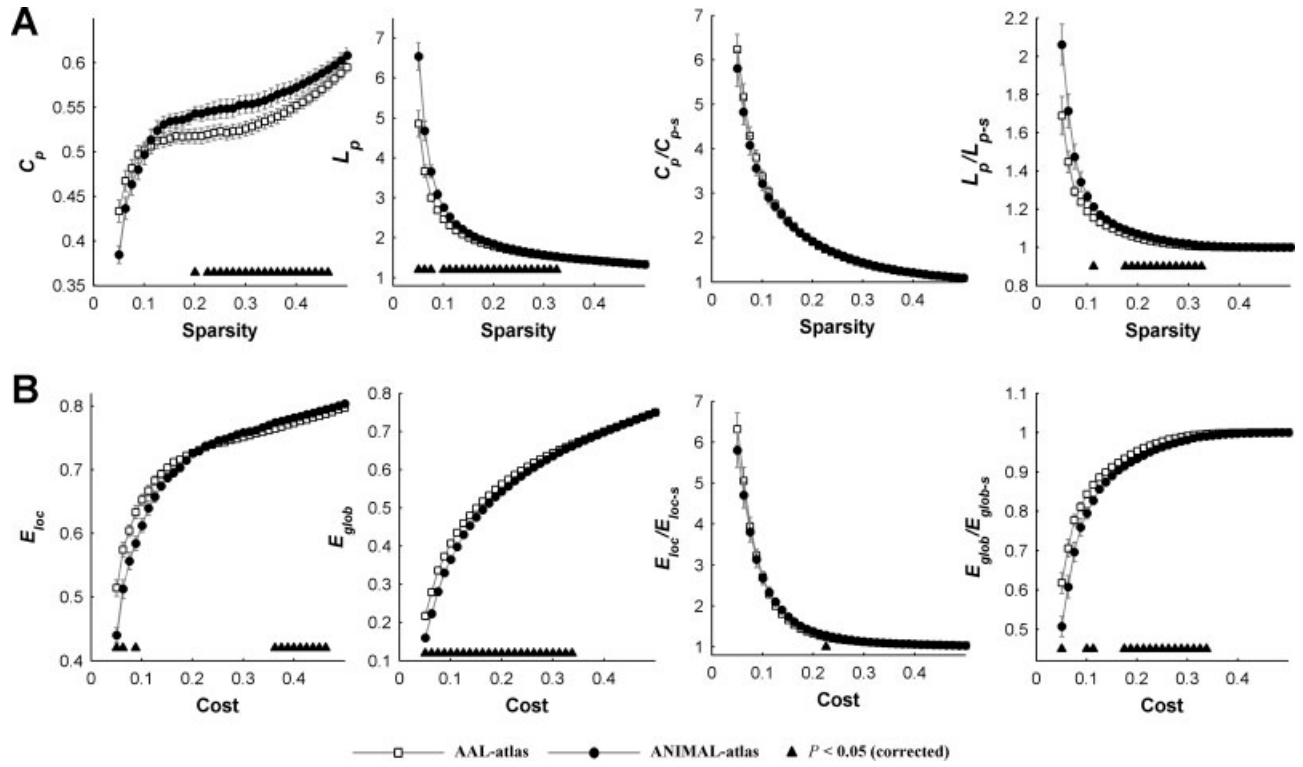

Figure 1.

Small-world measurements of brain functional networks using the AAL-atlas and ANIMAL-atlas as a function of threshold. Error bars correspond to standard error of the mean over subjects. **A**: conventional small-world parameters as a function of sparsity threshold, S (from left to right, clustering coefficient, C_p, characteristic path length, L_p, scaled clustering coefficient, $C_p/C_{p\text{-}s}$, and scaled path length, $L_p/L_{p\text{-}s}$, by 100 degree-matched random networks); **B**: small-world efficiency parameters as a function of cost threshold, K (from left to right, local efficiency, E_{loc}, global efficiency, E_{glob}, scaled local efficiency, $E_{loc}/E_{loc\text{-}s}$, and scaled global efficiency, $E_{glob}/E_{glob\text{-}s}$, by 100 degree-matched random networks). The black triangles indicate that there are significant between-atlas differences in the topological parameters of functional brain networks ($P < 0.05$, corrected).

RESULTS

Small-World Brain Functional Networks

Small-world properties

Conventional network analysis showed both AAL-atlas- and ANIMAL-atlas-based functional brain networks had a small-world topology ($C_p/C_{p\text{-}s} > 1$ and $L_p/L_{p\text{-}s} \approx 1$, Fig. 1A) over a wide range of sparsity ($0.05 \leq S \leq 0.5$). The network efficiency analysis also demonstrated the small-world configurations ($E_{loc}/E_{loc\text{-}s} > 1$ and $E_{loc}/E_{loc\text{-}s} \approx 1$, Fig. 1B) over a wide range of cost ($0.05 \leq K \leq 0.5$). Both results are consistent with previous functional brain network studies (Achard et al., 2006; Achard and Bullmore, 2007; Salvador et al., 2005; Wang et al., in press). To further assess whether the small-world attributes shown here also exist at brain networks with other sizes (i.e. the number of nodes), in the present study, we recalculated the small-world parameters of simulated brain networks with 50, 30, and 20 regions, respectively, which were obtained by a randomized merging algorithm (for details, see the legend of Fig. 2). The results indicated that all of the simulated networks had small-world topology as those real brain networks, i.e., $C_p/C_{p\text{-}s} > 1$ and $L_p/L_{p\text{-}s} \approx 1$, and $E_{loc}/E_{loc\text{-}s} > 1$ and $E_{glob}/E_{glob\text{-}s} \approx 1$ (see Fig. 2). Taken together, human brain functional networks exhibit robust small-world properties at a regional level, regardless of the selection of brain atlases or network size applied.

Parcellation-related small-world differences between groups

Statistical analysis revealed significant differences in C_p within a wide range of sparisty ($0.2 < S < 0.46$) between the two groups of real brain networks (Fig. 1A). However, when scaled to degree-matched random networks ($C_p/C_{p\text{-}s}$), these differences disappeared. Furthermore, we found that there were significant differences in both L_p ($0.05 < S < 0.32$) and $L_p/L_{p\text{-}s}$ ($0.17 < S < 0.32$) between the two groups (Fig. 1A). Figure 1B showed the comparisons of network

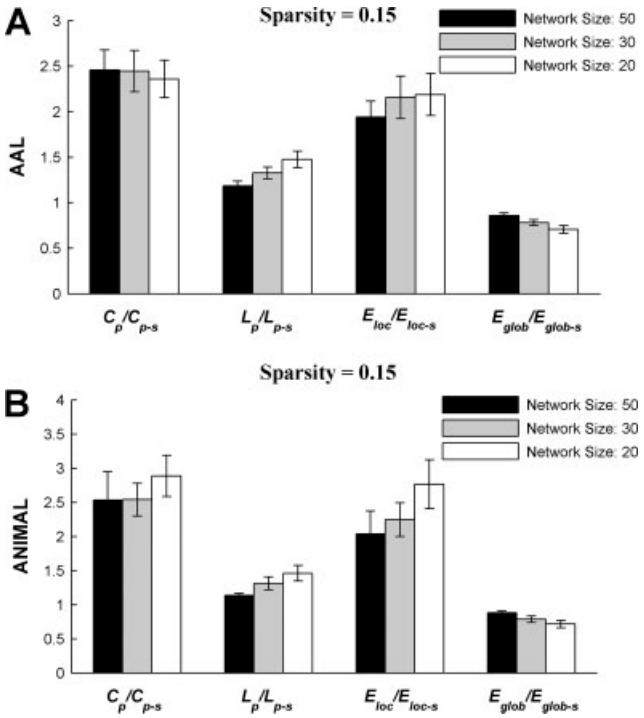

Figure 2.

Small-world properties of simulated brain networks with different sizes. The networks were obtained by a randomized merging algorithm in which multiple different brain regions were merged into one single region. The process was briefly described as follows. First, one region was randomly chosen from a prior brain atlas. This region was then merged with one of its neighbors into a new one. This procedure was repeatedly performed until the resulting network had a size of 50, 30, and 20 regions, respectively. Finally, small-world properties of the resulting networks were analyzed by using graph theoretical approaches. It was noted that, at a certain network size, the small-world parameters were calculated by averaging 20 merged networks with the same size. Our results indicated that all of the simulated networks at $S = 0.15$ met the conditions, $C_p/C_{p\text{-}s} > 1$, $L_p/L_{p\text{-}s} \approx 1$ and $E_{loc}/E_{loc\text{-}s} > 1$, $E_{glob}/E_{glob\text{-}s} \approx 1$ for the AAL-atlas (**A**) and ANIMAL-atlas (**B**), which suggests that large-scale brain functional networks had robust small-world architecture at different spatial scales. The similar results were also found at $S = 0.10$ and 0.20 (data not shown).

efficiency between the two groups and significant parcellation-related differences were observed in E_{loc} ($0.36 < K < 0.46$), E_{glob} ($0.05 < K < 0.32$) and $E_{glob}/E_{glob\text{-}s}$ ($0.17 < K < 0.34$) (Fig. 1B). The results of network efficiency were largely compatible with the conventional small-world results. Finally, the "energy" comparisons of functional networks revealed significant between-group differences ($P < 0.05$) in the area under the C_p, L_p, $L_p/L_{p\text{-}s}$, E_{glob} and $E_{glob}/E_{glob\text{-}s}$ curves or trend ($P = 0.07$) in the area under the E_{loc} curve, whereas area under the $C_p/C_{p\text{-}s}$ and $E_{loc}/E_{loc\text{-}s}$ curves did not show significant differences (see Fig. 3).

Parcellation-Related Degree Distribution Differences Between Groups

Degree distribution of both AAL-atlas- and ANIMAL-atlas-based brain functional networks followed an exponentially truncated power law model, $P(k) \sim k^{\alpha-1}e^{-k/kc}$ (α is an estimated exponent and k_c is a cutoff degree) as opposed to a scale-free regime (see Fig. 4). The results are consistent with previous structural and functional brain networks studies using the AAL-atlas (Achard et al., 2006; Iturria-Medina et al., 2008; Wang et al., in press) and the ANIMAL-atlas (He et al., 2007). Figure 4 also showed the fitting results of one representative subject at $S = 0.1$, 0.15 and 0.2, respectively. Further statistical evaluation revealed significant differences ($P < 0.05$) or trends ($0.05 < P < 0.1$) in both α and k_c between the two groups (see Fig. 5), sug-

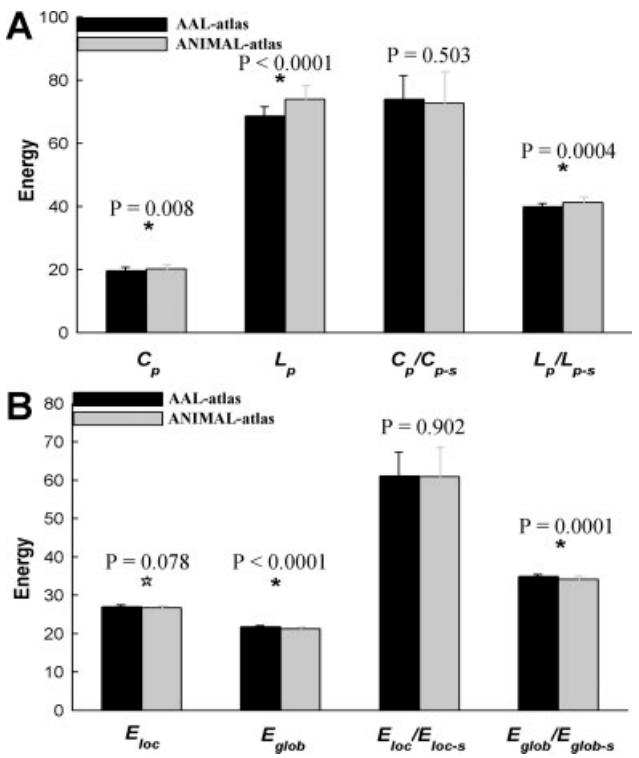

Figure 3.

Small-world energy of brain functional networks using the AAL-atlas and ANIMAL-atlas. Here, "energy" means the areas under the curves of corresponding parameters. **A**: "energy" of conventional small-world parameters; **B**: "energy" of small-world efficiency parameters. Error bars correspond to standard deviation of the mean across participants, and *P* values are the significance of the statistical comparison using paired *t* tests. Note that the asterisk indicates $P < 0.05$, and the five-pointed star indicates $0.05 < P < 0.01$.

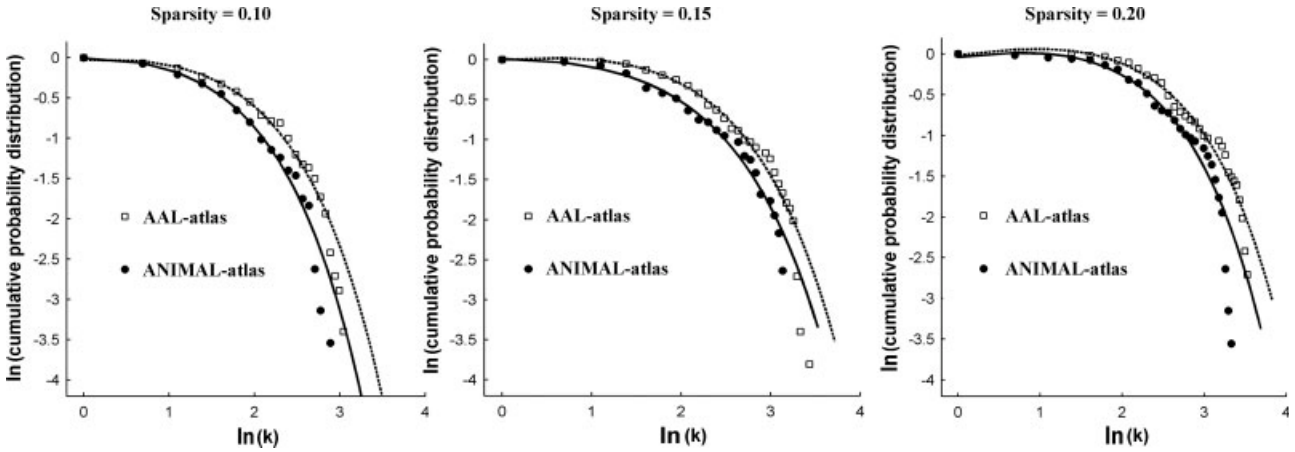

Figure 4.

Degree distribution of human brain functional networks. The networks were derived from a representative participant at a sparsity threshold of 0.10, 0.15, and 0.20. Plot of the ln of the cumulative probability of degree, ln ($P(k)$), versus log of degree, ln (k). The open squares signs indicate the observed data from the AAL atlas, and black solid circles show the observed data from the ANIMAL atlas.

gesting parcellation-related between-group differences in degree distribution parameters.

The Relation Between Nodal Properties and Regional Size

In the present study, we also examined the relationship between the size of brain regions and their network indices (degree k_{nodal}, nodal cluster coefficient $C_{p\text{-}nodal}$, nodal local efficiency $E_{loc\text{-}nodal}$, and nodal efficiency E_{nodal}, see Table III for the details of the nodal indices) at $S = 0.10$, 0.15, and 0.20, respectively. For the AAL atlas, both k_{nodal} (at $S = 0.20$) and E_{nodal} (at $S = 0.15$ and 0.20) were found to be positively correlated with the regional size. However, we found that both $E_{loc\text{-}nodal}$ (at $S = 0.10$) and $C_{p\text{-}nodal}$ (at $S = 0.10$, 0.15, and 0.20) had negative correlations with the regional size. For the ANIMAL atlas, all measures (k_{nodal}, $C_{p\text{-}nodal}$, $E_{loc\text{-}nodal}$, and E_{nodal}) had significantly negative correlations with the regional size at each selected threshold (see Fig. 6).

DISCUSSION

In this study, we investigated the important issue of the influences of different atlas-based parcellation schemes on topological properties of human brain functional networks using resting-state fMRI. Our results showed that brain functional networks had robust small-world properties and truncated power-law degree distribution regardless of the selection of different atlases. However, significant between-group differences were observed in both local (C_p and E_{loc}) and global (L_p, $L_p/L_{p\text{-}s}$, E_{glob}, and $E_{glob}/E_{glob\text{-}s}$) features of the networks. These results provided, for the first time, quantitative evidences of the parcellation-dependent topological parameters in the human brain functional networks.

Conventional Small-World Parameters and Network Efficiency

We found robust small-world attributes in both brain functional networks constructed from the two different

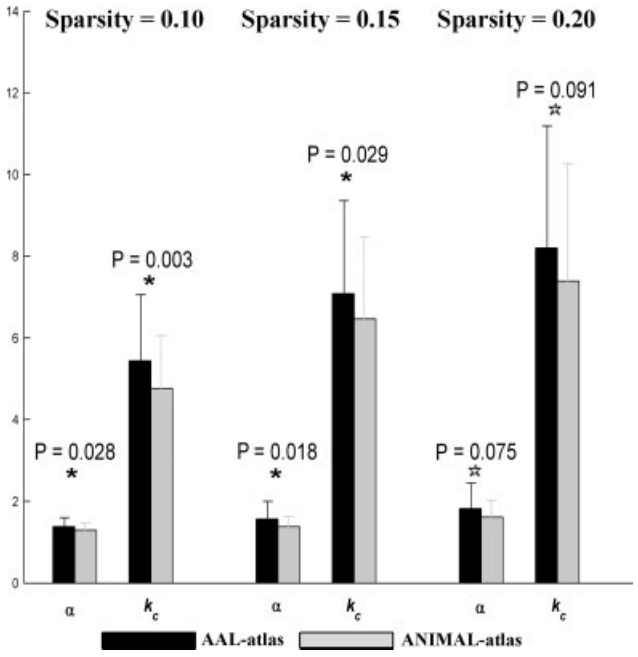

Figure 5.

Barplot showing the mean and standard deviation of fitting constant components α and k_c across subjects at a sparsity threshold of 0.10, 0.15, and 0.20. These threshold values correspond to those of Figure 3. P values show significant differences (asterisk) or trends (five-pointed star) between the two groups, which are obtained by using paired t tests.

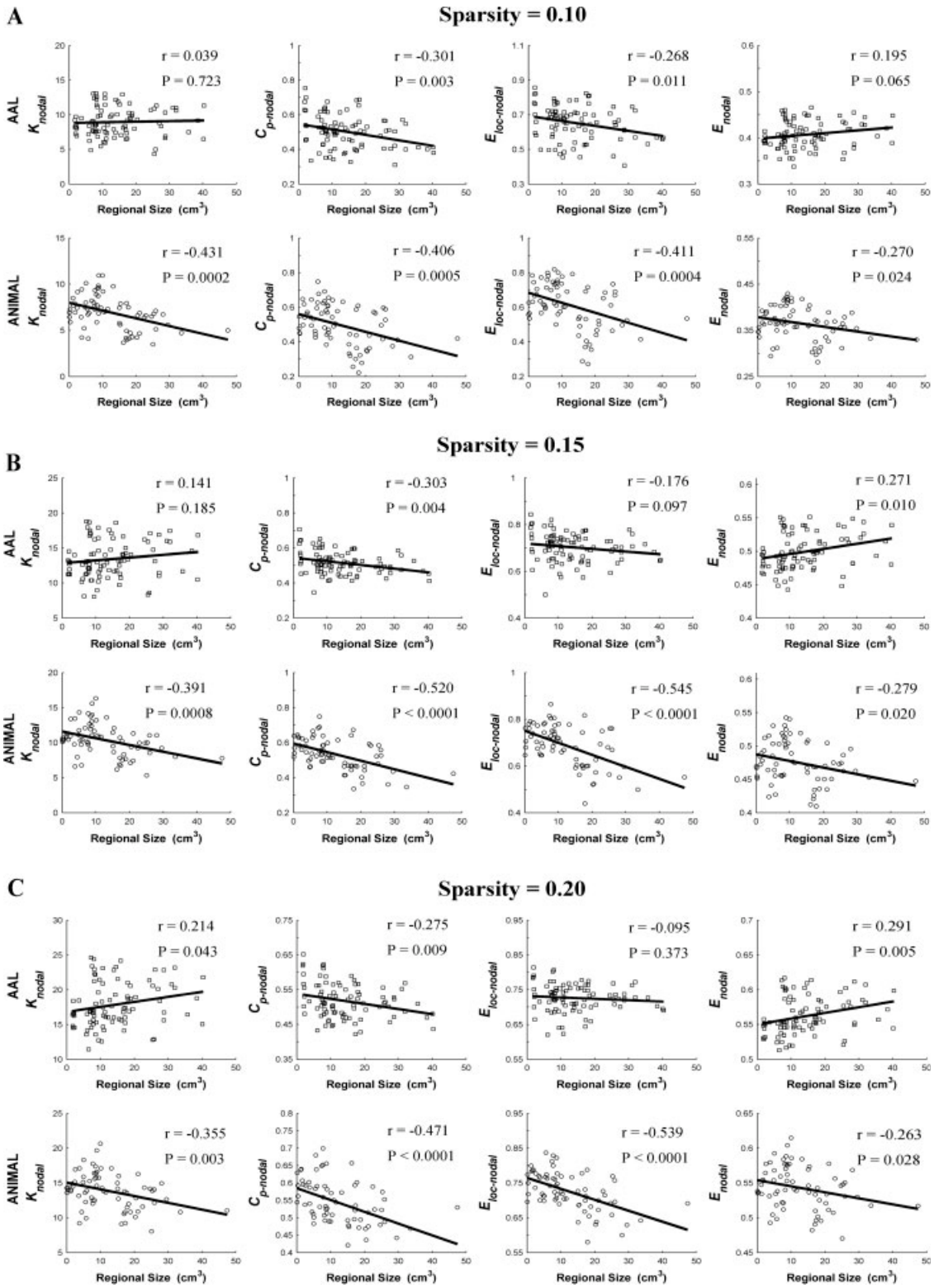

Figure 6.

The relation between the regional size and nodal properties of brain networks. The nodal properties used in this study included degree, k_{nodal}, clustering coefficient, $C_{p\text{-}nodal}$, local efficiency, $E_{loc\text{-}nodal}$, and nodal efficiency, E_{nodal} (for the descriptions of the parameters, see Table III). It was noted that, for the two atlases (AAL and ANIMAL), the brain networks were constructed at $S = 0.10$ (**A**), 0.15 (**B**), and 0.20 (**C**), respectively. The solid lines were obtained by a linear regression of nodal indices on regional size. r and P values represent correlation coefficients and the corresponding significant levels (uncorrected), respectively.

parcellation atlases (AAL-atlas and ANIMAL-atlas). Our findings are in accordance with several recent studies showing small-world properties in functional brain networks based on the AAL-atlas (Achard et al., 2006; Achard and Bullmore, 2007; Salvador et al., 2005; Wang et al., in press). It is worthwhile to note that although the ANIMAL atlas was previously implemented in the structural brain networks analysis (He et al. 2007), it has never been applied in any functional brain networks analysis prior to this study. Here, we demonstrated for the first time that functional brain networks based on the ANIMAL-atlas also displayed robust small-world attributes. Using computation simulation approaches, Sporns et al. (2000) found that small-world topology emerges when networks are evolved into an optimal balance between local specialization and global integration. Thus, our results provide further support the hypothesis that the human brain has evolved into an optimal fashion to maximize the efficiency of information processing and minimize required wiring costs (for a review, see Bassett and Bullmore, 2006). Additionally, we also noted (although grossly) that there were the trends in the small-world parameters as a function of network size, e.g., $L_p/L_{p\text{-}s}$ increases as the number of the network nodes decreases (see Fig. 2). In future, it would be interesting to further explore the relation between the topological parameters and network size.

Despite the common small-world topology, in the present study, we found significant differences in both local (C_p and E_{loc}) and global (L_p, $L_p/L_{p\text{-}s}$, E_{glob}, and $E_{glob}/E_{glob\text{-}s}$) topological attributes between the two groups of brain functional networks (see Fig. 1). The results strongly indicate that most small-world parameters are sensitive to the selection of the parcellation atlases. The observed differences might be attributed to several potential sources: (1) different processes applied in generating the atlases. Although both AAL and ANIMAL atlases were completely depicted in terms of macroscopic surface features (i.e., sulcal pattern), the detailed processes are different: sulcal patterns of AAL-atlas were obtained automatically via software, while boundaries of brain structures from ANIMAL-atlas were all manually chosen with reference to various atlases introduced by Ono et al. (1990) and Talairach and Tournoux (1988). This methodological diversity might result in the differences of precision and accuracy in the segmentation process, e.g., the size and shape of brain regions; (2) different network sizes (AAL: 90; ANIMAL: 70). From a network aspect, the characterization of its properties (e.g., small-worldness) is associated with the network size and connections. A change in the network size and connections might result in the alterations of topological architecture of the graphs and inevitably cause the changes in the network properties. Together, all these presumptions may account for, to a certain extent, the observed between-group differences in certain network attributes. Interestingly, despite the parcellation-related differences in C_p and E_{loc}, the ratios of $C_p/C_{p\text{-}s}$ and $E_{loc}/E_{loc\text{-}s}$ were not affected, which could be attributed to the similar changes in network properties of the corresponding degree-matched random networks.

Degree Distribution

The small-world brain functional networks have been found to have different connectivity degree distribution. For example, Eguiluz et al. (2005) found that human brain functional networks derived from experimentally activated fMRI data at a mesoscale (voxel level) had a scale-free (i.e., power law) degree distribution, while studies from Achard et al. (2006) and Wang et al. (in press) showed that functional networks of the human brain derived from resting-state fMRI data at a macroscale (regional level) followed an exponentially truncated power law distribution. This discrepancy of degree distribution may be associated with the spatial scale at which the functional networks were constructed. Here, at macroscale, we also demonstrated an exponentially truncated power law distribution for the two groups of brain functional networks that are in accordance with previous functional brain network studies (Achard and Bullmore, 2007; Wang et al., in press). The exponentially truncated power law degree distribution implied that the functional brain networks permitted the existence of some core regions but prevented the emergence of huge hubs with a large number of edges. Compared with a scale-free network, an exponentially truncated power law distribution network conferred distinctive advantages in the light of robustness to both random elimination of nodes (brain regions) and selective attack on hubs (Achard et al., 2006; Albert et al., 2000). Hence, we inferred that this robustness facilitated the ability of brain to withstand the regional lesions of network functionality in the face of developmental aberration or disease (Achard et al., 2006). The appearance of such network structure may be attributed to the physical constraints on the brain network growing process such as aging of the brain regions and cost of adding connections to the regions (Albert and Barabasi, 2002; Amaral et al., 2000). However, we did observed significant differences or trends in the fitting components α and k_c (see Fig. 4) between the two groups. The component α reflects the extent of node degrees distribution within a network and k_c is a critical value. The differences in the degree fitting parameters suggest that brain parcellation schemes have wide influences on the network topology, such as the distribution of core nodes.

The Relation Between Nodal Properties and Regional Size

Recently, Salvador et al. (2008) showed that regional volume had a positive correlation with its mutual information (MI) that measured the functional connectivity between the region and the rest brain regions. In the present study, we noted that, for the AAL atlas, k_{nodal} and E_{nodal} were positively correlated with the regional size at several threshold levels, which is in accordance with the previous

study (Salvador et al., 2008). However, we also noted inconsistent results. For instance, all nodal measures in the ANIMAL atlas showed negative correlations with the regional size (see Fig. 6). The discrepancies among these results could be attributed to (1) different nodal attributes used in the studies [multiple nodal parameters in this study (Table III) vs. MI in the Salvador's study], and (2) different regional parcellation strategies applied in the two brain atlases as described previously. Despite the discrepancies in the results, our study pointed to a clear effect of regional size on the small-world analysis. It implies that, while performing topological analyses on the brain networks that are constructed from the anatomical atlases, the effects of regional size need to be taken into account in the future.

Further Considerations

Our results have important implications in characterizing parcellation-related topological alterations of large-scale brain networks. Many previous studies using neurophysiological and neuroimaging data have demonstrated small-world alterations in development (Micheloyannis et al., in press), normal aging (Achard and Bullmore, 2007) and brain disorders (Bartolomei et al., 2006; He et al., 2008; Liu et al., 2008; Micheloyannis et al., 2006b; Ponten et al., 2007; Rubinov et al., in press; Stam et al., 2007; Wang et al., in press). However, some of these studies did not find significant differences in several specific small-world parameters, such as the clustering coefficient (Stam et al., 2007), path length (Ferri et al., 2007), or global efficiency (De Vico Fallani et al., 2007; Wang et al., in press). According to our results, one could therefore suspect that the nonsignificant results shown in the previous studies could be due to the different regional parcellation methods they used. Our study thus provides implications for the choice of parcellation strategies in the future researches.

Several issues remain to be addressed. First, in this study, the two adopted atlases were obtained according to sulcal patterns from only one subject; so it was unsuitable to apply them to a group-level analysis due to interindividual variability of anatomical structures. Given the variations in sulcal pattern are associated with the location and geometry between individuals (Thompson et al., 1996), it would be interesting to apply a probabilistic atlas of human brain to regional parcellation or define individual brain regions through a combination of diffusion tensor imaging with fMRI (Sporns et al., 2005). Second, the head motion of subjects might have confounding effects on the final results of network analysis. Recently, Salvador et al. (2008) found that the residual effects of head motion were associated with the functional connectivity of many brain regions at high frequencies (0.17–0.25 Hz), but there were no strong linear correlations with that at middle (0.08–0.17 Hz) and low (<0.08 Hz) frequencies. To examine whether the results of our network analysis were affected by the head motion, in the present study, we also calculated the correlation between the average values of head movement (absolute translations in x, y, and z separately) and small-world parameters of brain networks by using a multivariate model (Salvador et al., 2008). Our results showed no significant correlations ($P > 0.05$) between the head motion and the parameters (C_p, $C_p/C_{p\text{-}s}$, L_p, $L_p/L_{p\text{-}s}$, E_{loc}, $E_{loc}/E_{loc\text{-}s}$, E_{glob}, and $E_{glob}/E_{glob\text{-}s}$) of brain networks that were derived from low-frequency (0.01–0.10 Hz) fMRI signals, which was consistent with Salvador et al.'s study (2008). Third, all of the network measurements used in this study were on the basis of binarized graphs that were constructed by thresholding the functional connectivity matrices. Though the use of binarized graphs reduced the complexity of network analysis, it also removed some detailed information. Further work could be conducted by using continuous weighted correlation values in the construction of brain networks (Achard et al., 2006; Jiang et al. 2004; Latora and Marchiori, 2003).

CONCLUSION

In this study, we quantitatively analyzed the influences of anatomical atlases on topological attributes of human brain functional networks acquired from resting-state fMRI. Our results indicated that, although the brain networks had robust small-world configuration and followed an exponentially truncated power law distribution under different atlases parcellation strategies, there were significantly between-atlas differences in both local and global topological parameters. These findings provide direct evidences on how functional topological properties of brain networks are associated with network node definition. The present study might have important implications in large-scale structural and functional brain networks studies under normal and pathological conditions.

ACKNOWLEDGMENTS

We would like to thank two anonymous reviewers for their thoughtful comments.

REFERENCES

Achard S, Bullmore E (2007): Efficiency and cost of economical brain functional networks. PLoS Comput Biol 3:e17.

Achard S, Salvador R, Whitcher B, Suckling J, Bullmore E (2006): A resilient, low-frequency, small-world human brain functional network with highly connected association cortical hubs. J Neurosci 26:63–72.

Albert R, Barabasi A-L (2002): Statistical mechanics of complex networks. Rev Mod Phys 74:47.

Albert R, Jeong H, Barabasi A-L (2000): Error and attack tolerance of complex networks. Nature 406:378–382.

Amaral LA, Scala A, Barthelemy M, Stanley HE (2000): Classes of small-world networks. Proc Natl Acad Sci USA 97:11149–11152.

Ashburner J, Friston KJ (1999): Nonlinear spatial normalization using basis functions. Hum Brain Mapp 7:254–266.

Bartolomei F, Bosma I, Klein M, Baayen JC, Reijneveld JC, Postma TJ, Heimans JJ, van Dijk BW, de Munck JC, de Jongh A, Cover KS, Stam CJ (2006): Disturbed functional connectivity in brain tumour patients: evaluation by graph analysis of synchronization matrices. Clin Neurophysiol 117:2039–2049.

Bassett DS, Bullmore E (2006): Small-world brain networks. Neuroscientist 12:512–523.

Bassett DS, Meyer-Lindenberg A, Achard S, Duke T, Bullmore E (2006): Adaptive reconfiguration of fractal small-world human brain functional networks. Proc Natl Acad Sci USA 103:19518–19523.

Biswal B, Yetkin FZ, Haughton VM, Hyde JS (1995): Functional connectivity in the motor cortex of resting human brain using echo-planar MRI. Magn Reson Med 34:537–541.

Boccaletti S, Latora V, Moreno Y, Chavez M, Hwang DU (2006): Complex networks: Structure and dynamics. Phys Rep 424:175–308.

Chen ZJ, He Y, Rosa-Neto P, Germann J, Evans AC: Revealing modular architecture of human brain structural networks by using cortical thickness from MRI. Cereb Cortex (in press).

Collins DL, Holmes CJ, Peters TM, Evans AC (1995): Automatic 3-D model-based neuroanatomical segmentation. Hum Brain Mapp 3:190–208.

De Vico Fallani F, Astolfi L, Cincotti F, Mattia D, Marciani MG, Salinari S, Kurths J, Gao S, Cichocki A, Colosimo A, Babiloni F (2007): Cortical functional connectivity networks in normal and spinal cord injured patients: Evaluation by graph analysis. Hum Brain Mapp 28:1334–1346.

Eguiluz VM, Chialvo DR, Cecchi GA, Baliki M, Apkarian AV (2005): Scale-free brain functional networks. Phys Rev Lett 94:018102.

Ferri R, Rundo F, Bruni O, Terzano MG, Stam CJ (2007): Small-world network organization of functional connectivity of EEG slow-wave activity during sleep. Clin Neurophysiol 118:449–456.

Fox MD, Snyder AZ, Vincent JL, Corbetta M, Van Essen DC, Raichle ME (2005): The human brain is intrinsically organized into dynamic, anticorrelated functional networks. Proc Natl Acad Sci USA 102:9673–9678.

Fox MD, Snyder AZ, Vincent JL, Raichle ME (2007): Intrinsic fluctuations within cortical systems account for intertrial variability in human behavior. Neuron 56:171–184.

Friston KJ, Frith CD, Liddle PF, Frackowiak RS (1993): Functional connectivity: The principal-component analysis of large (PET) data sets. J Cereb Blood Flow Metab 13:5–14.

Friston KJ, Frith CD, Frackowiak RS, Turner R (1995): Characterizing dynamic brain responses with fMRI: A multivariate approach. Neuroimage 2:166–172.

Hagmann P, Kurant M, Gigandet X, Thiran P, Wedeen VJ, Meuli R, Thiran JP (2007): Mapping human whole-brain structural networks with diffusion MRI. PLoS ONE 2:e597.

He Y, Chen ZJ, Evans AC (2007): Small-world anatomical networks in the human brain revealed by cortical thickness from MRI. Cereb Cortex 17:2407–2419.

He Y, Chen ZJ, Evans AC (2008): Structural insights into aberrant topological patterns of large-scale cortical networks in Alzheimer's disease. J Neurosci 28:4756–4766.

Iturria-Medina Y, Sotero RC, Canales-Rodriguez EJ, Aleman-Gomez Y, Melie-Garcia L (2008): Studying the human brain anatomical network via diffusion-weighted MRI and graph theory. NeuroImage 40:1064–1076.

Jiang T, He Y, Zang Y, Weng X (2004): Modulation of functional connectivity during the resting state and the motor task. Hum Brain Mapp 22:63–71.

Kabani NJ, Collins DL, Evans AC (1998): A 3d neuroanatomical atlas. Presented at the 4th International Conference on Functional Mapping of the Human Brain, Montreal, Quebec, Canada, 7–12 June 1998.

Kiviniemi V, Jauhiainen J, Tervonen O, Paakko E, Oikarinen J, Vainionpaa V, Rantala H, Biswal B (2000): Slow vasomotor fluctuation in fMRI of anesthetized child brain. Magn Reson Med 44:373–378.

Latora V, Marchiori M (2001): Efficient behavior of small-world networks. Phys Rev Lett 87:198701.

Latora V, Marchiori M (2003): Economic small-world behavior in weighted networks. Eur Phys J B 32:249–263.

Liu Y, Liang M, Zhou Y, He Y, Yu CS, Song M, Liu HH, Liu ZN, Jiang TZ (2008): Disrupted small-world networks in schizophrenia. Brain 131:945–961.

Lowe MJ, Mock BJ, Sorenson JA (1998): Functional connectivity in single and multislice echoplanar imaging using resting-state fluctuations. Neuroimage 7:119–132.

Maslov S, Sneppen K (2002): Specificity and stability in topology of protein networks. Science 296:910–913.

Micheloyannis S, Pachou E, Stam CJ, Vourkas M, Erimaki S, Tsirka V (2006a): Using graph theoretical analysis of multi channel EEG to evaluate the neural efficiency hypothesis. Neurosci Lett 402:273–277.

Micheloyannis S, Pachou E, Stam CJ, Breakspear M, Bitsios P, Vourkas M, Erimaki S, Zervakis M (2006b): Small-world networks and disturbed functional connectivity in schizophrenia. Schizophr Res 87:60–66.

Micheloyannis S, Vourkas M, Tsirka V, Karakonstantaki E, Kanatsouli K, Stam CJ: The influence of ageing on complex brain networks: A graph theoretical analysis. Hum Brain Mapp (in press).

Newman MEJ (2003): The structure and function of complex networks. SIAM Rev 45:167–256.

Ono M, Kubik S, Abernathey CD (1990): Atlas of the Cerebral Sulci. New York: Thieme.

Ponten SC, Bartolomei F, Stam CJ (2007): Small-world networks and epilepsy: Graph theoretical analysis of intracerebrally recorded mesial temporal lobe seizures. Clin Neurophysiol 118:918–927.

Rubinov M, Knock SA, Stam CJ, Micheloyannis S, Harris AW, Williams LM, Breakspear M: Small-world properties of nonlinear brain activity in schizophrenia. Hum Brain Mapp (in press).

Salvador R, Suckling J, Coleman MR, Pickard JD, Menon D, Bullmore E (2005): Neurophysiological architecture of functional magnetic resonance images of human brain. Cereb Cortex 15:1332–1342.

Salvador R, Martinez A, Pomarol-Clotet E, Gomar J, Vila F, Sarro S, Capdevila A, Bullmore E (2008): A simple view of the brain through a frequency-specific functional connectivity measure. Neuroimage 39:279–289.

Sporns O, Zwi JD (2004): The small world of the cerebral cortex. Neuroinformatics 2:145–162.

Sporns O, Tononi G, Edelman GM (2000): Theoretical neuroanatomy: relating anatomical and functional connectivity in graphs and cortical connection matrices. Cereb Cortex 10:127–141.

Sporns O, Tononi G, Kotter R (2005): The human connectome: A structural description of the human brain. PLoS Comput Biol 1:e42.

Stam CJ (2004): Functional connectivity patterns of human magnetoencephalographic recordings: A 'small-world' network? Neurosci Lett 355:25–28.

Stam CJ, Reijneveld JC (2007): Graph theoretical analysis of complex networks in the brain. Nonlinear Biomed Phys 1:3.

Stam CJ, Jones BF, Nolte G, Breakspear M, Scheltens P (2007): Small-world networks and functional connectivity in Alzheimer's disease. Cereb Cortex 17:92–99.

Talairach J, Tournoux P (1988): Co-Planar Stereotaxic Atlas of the Human Brain. New York: Thieme.

Thompson PM, Schwartz C, Lin RT, Khan AA, Toga AW (1996): Three-dimensional statistical analysis of sulcal variability in the human brain. J Neurosci 16:4261–4274.

Tzourio-Mazoyer N, Landeau B, Papathanassiou D, Crivello F, Etard O, Delcroix N, Mazoyer B, Joliot M (2002): Automated anatomical labeling of activations in SPM using a macroscopic anatomical parcellation of the MNI MRI single-subject brain. Neuroimage 15:273–289.

Wang L, Zhu CZ, He Y, Zang YF, Cao QJ, Zhang H, Zhong QH, Wang YF: Altered small-world brain functional networks in children with attention-deficit/hyperactivity disorder. Hum Brain Mapp (in press).

Watts DJ, Strogatz SH (1998): Collective dynamics of 'small-world' networks. Nature 393:440–442.